Journal of Luminescence 153 (2014) 221–226

Contents lists available at ScienceDirect

Journal of Luminescence

journal homepage: www.elsevier.com/locate/jlumin

Spectroscopic and photoluminescence characterization of Eu^{3+}-doped monoclinic $KY(WO_4)_2$ crystal

P.A. Loiko [a], V.I. Dashkevich [b], S.N. Bagaev [c], V.A. Orlovich [b], A.S. Yasukevich [a], K.V. Yumashev [a,*], N.V. Kuleshov [a], E.B. Dunina [d], A.A. Kornienko [d], S.M. Vatnik [c], A.A. Pavlyuk [e]

[a] Center for Optical Materials and Technologies, Belarusian National Technical University, 65/17 Nezavisimosti Avenue, Minsk 220013, Belarus
[b] B.I. Stepanov Institute of Physics, NAS of Belarus, 68 Nezavisimosti Avenue, Minsk 220072, Belarus
[c] Institute of Laser Physics, SB of RAS, 13/3 Lavrentyev Avenue, Novosibirsk 630090, Russia
[d] Vitebsk State Technological University, 72 Moskovskaya Avenue, Vitebsk 210035, Belarus
[e] Nikolaev Institute of Inorganic Chemistry, SB of RAS, 3 Lavrentyev Avenue, Novosibirsk 630090, Russia

ARTICLE INFO

Article history:
Received 28 November 2013
Received in revised form
15 March 2014
Accepted 18 March 2014
Available online 26 March 2014

Keywords:
Double tungstates
Trivalent europium
Absorption
Photoluminescence
Red emission

ABSTRACT

Monoclinic 2 at% Eu-doped $KY(WO_4)_2$ is grown by top-seeded solution growth method. Polarization-resolved absorption and stimulated-emission cross-section spectra are determined for this crystal. Spectroscopic properties of Eu:$KY(WO_4)_2$ are modeled within conventional Judd–Ofelt theory, as well as theory of f–f transition intensities for systems with anomalously strong configuration interaction, yielding absorption oscillator strengths, luminescence branching ratios and radiative lifetime of $^5D_0$ state. The impact of excited-state absorption from this state on possibility of laser operation is discussed. Photoluminescent properties of Eu:$KY(WO_4)_2$ are determined. This crystal provides intense red emission with CIE coordinates $x=0.670$, $y=0.329$.

1. Introduction

Trivalent europium ions, Eu^{3+}, doped into crystalline and glassy materials, possess important applications in tricolor fluorescent lamps, field emission displays, cathode-ray tubes and solid-state lightning technologies. Europium-based phosphors allows one to obtain intense red emission near ~612 nm related with $^5D_0 \rightarrow {}^7F_2$ transition within $4f^6$ electronic shell. Today main commercial host for Eu^{3+} is yttrium oxide Y_2O_3 [1,2]; however, the search of novel inorganic hosts is still in progress. Particularly, europium-doped potassium and sodium double tungstates (DT) and double molybdates (DMo) are recognized as perspective red phosphors [3,4].

Eu^{3+} ion is also suitable for generation of red laser emission on above mentioned channel. Laser action was realized for the first time in bulk Y_2O_3 [5] and liquid chelat [6] at cryogenic temperature, later similar experiment was performed with Eu:YVO_4 [7]. Room-temperature (RT) lasing was obtained with Eu:GaN [8] and Eu:polymer [9] thin films. Recently, 25 at% Eu-doped potassium gadolinium DT, $KGd(WO_4)_2$, was introduced as novel bulk dielectric material for pulsed room-temperature Eu^{3+} lasing [10]. Specifically, it was realized on $^5D_0 \rightarrow {}^7F_4$ transition centered at ~702 nm.

Monoclinic DTs with common formula $KRE(WO_4)_2$ (KREW, with RE=Y, Gd, Lu) doped with variety of trivalent rare-earth ions are well-known materials for efficient solid-state lasers [11]. However, the spectroscopic and laser properties of Eu-doped monoclinic DTs are far from complete description. Under Eu doping, these ions enter positions of "passive" RE^{3+} ones, so no $Eu^{3+} \rightarrow Eu^{2+}$ reduction occurs. Recently, crystalline structure, cryogenic and RT absorption and PL properties were reported for 1.5–5 at% Eu:KLuW [12]. In Ref. [13], absorption and stimulated-emission cross-section spectra were evaluated for KGdW with higher Eu content, 10 at%. Bulk $KYb_{0.8}Eu_{0.2}W$ crystal was studied in Ref. [14]; however, main attention was paid to cooperative energy transfer between Yb^{3+} pairs and single Eu^{3+} ions. Some information about spectroscopic properties of Eu:KGdW, Eu:KYbW, KEuW and Eu:KGd(W/Mo) nanocrystalline phosphors was presented in Refs. [3,15–18].

* Corresponding author. Tel.: +375 17 293 9188; fax: +375 17 292 6286.
E-mail address: k.yumashev@tut.by (K.V. Yumashev).

http://dx.doi.org/10.1016/j.jlumin.2014.03.037
0022-2313/

Thus, important representative of monoclinic DTs family, Eu:KYW, is still uncharacterized.

In the present paper, we aimed to perform detailed spectroscopic investigation of 2 at% Eu:KYW, for the first time, to our knowledge. Polarization-resolved absorption and stimulated-emission cross-section spectra were evaluated; Judd–Ofelt theory and theory adopted for systems with anomalously strong configuration interaction were applied for determination of absorption oscillator strengths (including excited-state absorption processes), luminescence branching ratios and radiative lifetime of $^5D_0$ state. In addition, PL properties of Eu:KYW were thoroughly studied.

2. Experimental

Europium-doped potassium yttrium double tungstate Eu:KYW melts at ~1080 °C and near this temperature it has an orthorhombic structure (β-phase) similar to one of disordered double molybdates [19]. At the temperature of ~1020 °C this crystal undergoes phase transition to low-temperature monoclinic α-phase. Such α-Eu:KYW crystal in the present paper was grown from the flux under low thermal gradients (below 0.1 °C/cm); potassium ditungstate $K_2W_2O_7$ was used as a solvent. Seed crystals were oriented along [0 1 0] crystallographic axis. Content of Eu^{3+} ions was 2 at% ($N_{Eu}=1.26\times10^{-20}$ cm^3, crystal density $\rho=6.501$ g/cm^3); growth rate was 3–5 mm/day. Obtained ~150 g boule was ~60 mm along growth direction, with $\sim20\times20$ mm^2 edge face, Fig. 1. The background losses in the transparence region were below 0.005 cm^{-1}.

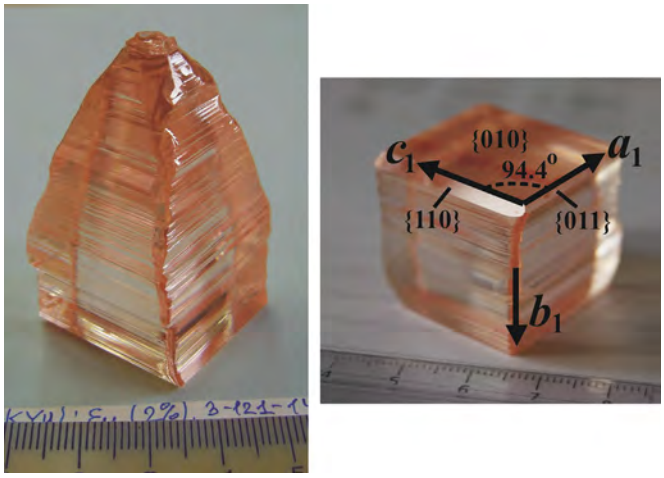

Fig. 1. As-grown crystal boule of 2 at% Eu:KY(WO$_4$)$_2$ (left image); habit of endface of this boule (right image): $\boldsymbol{a}_1$, $\boldsymbol{b}_1$ and $\boldsymbol{c}_1$ are the crystallographic axes, *I2/c* setting.

The crystal had weak rose coloration. With 2 at% of Eu, even large-volume boule was free of cracks and inclusions that is required for potential laser experiments (at higher Eu content, numerous cracks were observed in the as-grown crystal).

KYW is monoclinic (space group C^6_{2h}–*C2/c* [19]; however, for description of obtained habit of crystal boule, crystallographic setting *I2/c* is more applicable). Lateral sides of central (prismatic) part of the boule are determined by {1 1 0}, {0 1 1} faces and {1 0 0}, {0 0 1} pinacoids. The endface of the boule is mainly determined by well-developed pinacoid {0 1 0} that is surrounded with four relatively small {1 1 0}, {0 1 1} ones, see Fig. 1 (right image).

KYW is optically biaxial and its optical properties are described within the frame of optical indicatrix axes, namely N_p, N_m and N_g [20]. N_p axis coincides with crystallographic $\boldsymbol{b}$ axis, while N_m and N_g are positioned in the $\boldsymbol{a}$–$\boldsymbol{c}$ plane. For investigation of absorption and PL, one cubic sample with dimensions $7(N_p)\times11(N_m)\times10$ (N_g) mm^3 was prepared, with all of the faces polished. For determination of UV absorption edge, two 90 μm-thick polished slabs were prepared. They were cut in the N_p–N_g and N_m–N_g planes.

Polarized absorption spectra were measured on Varian CARY 5000 spectrophotometer in the UV, visible (0.3–0.7 μm, spectral bandwidth, SBW, was 0.06 nm) and near-IR (1.8–2.8 μm, SBW=0.1 nm). Photoluminescence (PL) was excited by focused radiation of 30 mW InGaN laser diode emitting near 400 nm. PL was collected in the direction perpendicular to the excitation one by a wide-aperture lens. The spectrum was registered by means of lock-in amplifier and monochromator MDR-23 (SBW~0.5 nm) with a Hamamatsu C5460-01 photodetector attached to its output slit. Glan–Taylor polarizer was placed before the input slit of monochromator.

For time-resolved PL studies, optical parametric oscillator Lotis TII LT-2214 tuned to 534 nm was used as an excitation source; the duration of excitation pulse was ~20 ns. PL was collected by wide-aperture lens and re-imaged to the input slit of monochromator MDR-12; then it was detected with fast Hamamatsu C5460 photodetector (40 ns response time) and 500 MHz Textronix TDS-3052B digital oscilloscope.

3. Results and discussion

Overview of absorption spectrum of 2 at% Eu:KYW crystal is presented in Fig. 2. The feature of Eu^{3+} ions is the close location of lower-lying excited multiplets, $^7F_1$ and $^7F_2$, to the ground-state one, $^7F_0$ (the energy gap is around 300 and 1000 cm^{-1}). The probability of their thermal population is high (0.33 and 0.02, as

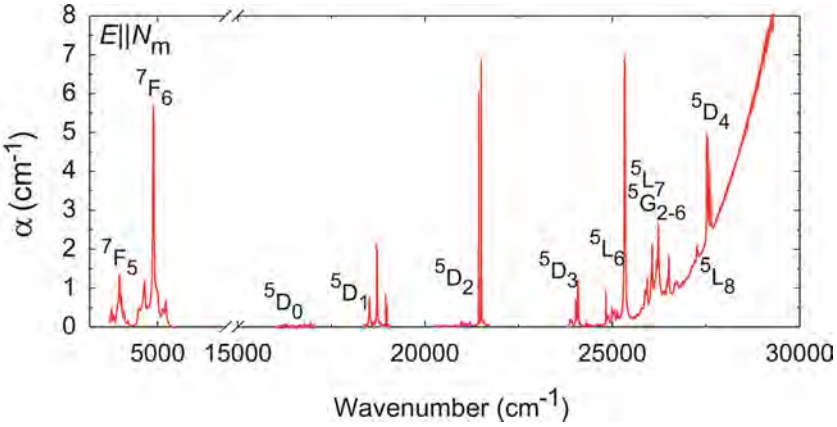

Fig. 2. Absorption spectrum of 2 at% Eu:KY(WO$_4$)$_2$ crystal (light polarization is $\boldsymbol{E}\|N_m$).

compared with 0.65 for ground-state), so transitions from ^7F_J (J=0, 1, 2) states are detected in the spectrum. Observed absorption bands in the visible and UV are related with transitions to higher-lying ^5D_J (J=0–4), ^5L_J (J=6–8) and ^5G_J (J=2–6) excited states. Characteristic bands of Eu^{3+} in the near-IR spanning across 1.8–2.8 μm range are related with transitions to lower-lying $^7F_5$ and $^7F_6$ excited states. Polarized structure of most intense and well-resolved absorption bands in the visible and near-IR is shown in Fig. 3 (for the exception of 0.3–0.4 μm spectral range that corresponds to intersection of levels from different multiplets, so exact assignment of each band is complicated).

Detailed analysis of absorption band related with $^7F_1 \rightarrow {}^5D_1$ transition is also presented in Table 1. This band is suitable for pumping of Eu:KYW with frequency-doubled Nd laser emitting around 532 nm [13]. Here λ_p is the peak wavelength; σ_{abs} is the corresponding peak absorption cross-section. Like other rare-earth-doped DTs [11], Eu:KGdW is characterized by strong anisotropy of optical absorption: maximum σ_{abs} corresponds to $\boldsymbol{E}\|N_m$; σ_{abs} for $\boldsymbol{E}\|N_p$ takes intermediate place; while $\boldsymbol{E}\|N_g$ is almost not suitable for pumping. Indeed, at λ_p=534.3 nm, $\sigma_{abs}(m):\sigma_{abs}(p):\sigma_{abs}(g)$=7.1:2.0:1. The anisotropy appears not only in intensity of absorption peaks, but also in their position. Indeed, the considered band for $\boldsymbol{E}\|N_p$ consists of three peaks (centered at 534.3, 538.9 and 540.0 nm); while for $\boldsymbol{E}\|N_m$ and N_g second peak is missing. This agrees with the fact that N_p axis coincides with C_2 symmetry axis of KYW lattice, while both N_m and N_g axes are positioned in the orthogonal plane [20]. Laser-pumping of Eu:KYW should be performed into the 534.3 nm peak for $\boldsymbol{E}\|N_m$ (in order obtain high pump efficiency). The main troubles here are moderate peak absorption ($\sigma_{abs}=1.71\times10^{-20}$ cm^2, or 2.2 cm^{-1} for 2 at% of Eu) and small full width at half maximum, FWHM, for this peak (~0.5 nm).

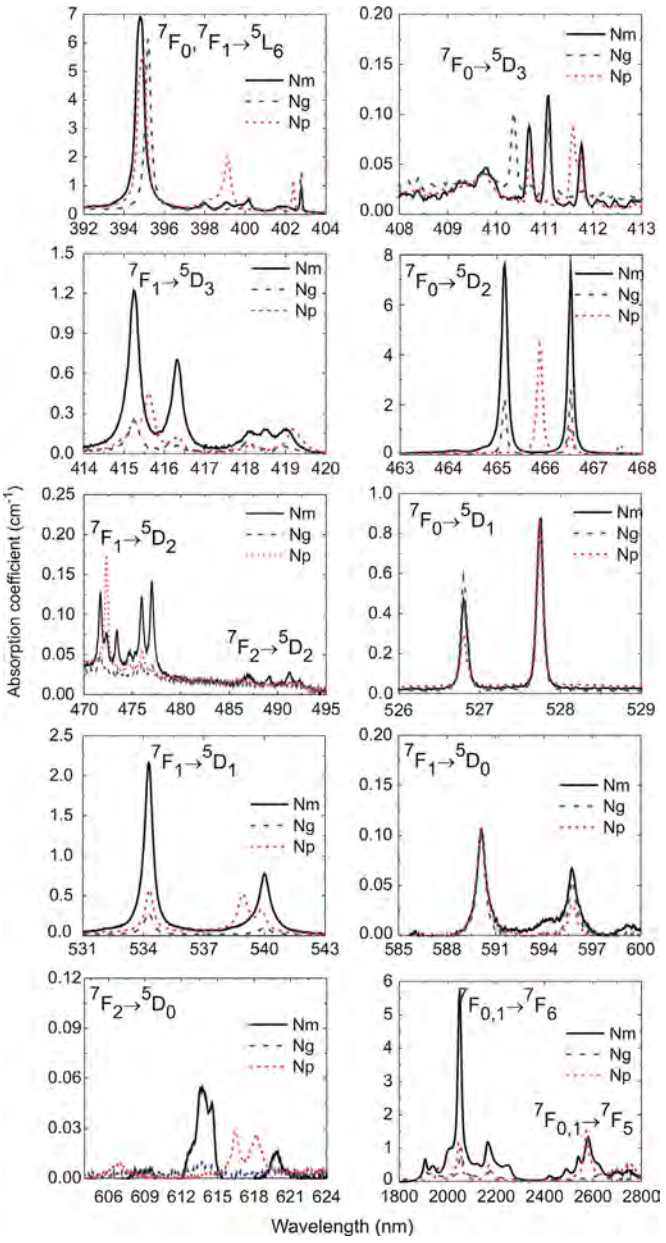

Fig. 3. Detailed structure of absorption bands for 2 at% Eu:KY(WO$_4$)$_2$ crystal in the visible (for principal light polarizations, $\boldsymbol{E}\|N_p$, N_m and N_g).

The position of UV absorption edge for 2 at% Eu:KYW slightly depends on light polarization, E_g=4.24÷4.32 eV (λ_g=287–292 nm), see Fig. 4, and is consistent with previous measurements for pure KYW [21].

Absorption oscillator strengths f for Eu^{3+} ion in KYW were determined directly from measured absorption spectrum $\alpha(\lambda)$

$$\langle f\rangle_{exp} = \frac{m_e c^2}{\pi e^2 N_{Eu} \bar{\lambda}^2} \int \alpha(\lambda) d\lambda, \quad (1)$$

where $\bar{\lambda}$ is the coordinate of "center of gravity" of selected absorption band (mean wavelength), N_{Eu} is the concentration of Eu^{3+} ions, m_e and e is the electron mass and charge, respectively, and the integration is performed within the spectral range covering the whole band. The brackets means that the values of f are averaged over three principal light polarizations

$$\langle f\rangle = \frac{1}{3}(f_p + f_m + f_g). \quad (2)$$

In addition, absorption oscillator strengths were calculated from line strength $S(JJ')$ modeled within conventional Judd–Ofelt (J–O) theory and theory of f–f transition intensities for systems with anomalously strong configuration interaction (ASCI) [22,23]

$$S_{J-O}(JJ') = \sum_k e^2 \Omega_k |\langle \gamma J|U^k|\gamma' J'\rangle|^2, \quad (3a)$$

$$S_{asci}(JJ') = \sum_k \frac{e^2}{4} |\langle \gamma J|U^k|\gamma' J'\rangle|^2 \times \left| O_{dk}\left(\frac{\Delta_d}{\Delta_d - E_J} + \frac{\Delta_d}{\Delta_d - E_{J'}}\right) + O_{ck}\left[\left(\frac{\Delta_{c1}}{\Delta_{c1} - E_J} + \frac{\Delta_{c1}}{\Delta_{c1} - E_{J'}}\right) + \left(\frac{\Delta_{c2}}{\Delta_{c2} - E_J} + \frac{\Delta_{c2}}{\Delta_{c2} - E_{J'}}\right) + \cdots\right]\right|^2. \quad (3b)$$

Here the summation is performed for k=2, 4, 6; $\langle \gamma J|U^k|\gamma' J'\rangle$ is the reduced matrix element of the unite matrix U^k, E_J and $E_{J'}$ are the energies of γJ and $\gamma' J'$ multiplets, {Ω_2, Ω_4 and Ω_6} are J–O parameters; while {O_{dk}, O_{ck}, Δ_d, Δ_{c1} and Δ_{c2}} refer to ASCI theory (parameter O_{dk} and energy Δ_d correspond to excited configuration of opposite parity $4f^{N-1}5d$, while O_{ck} and energies Δ_c correspond to covalent effects of excited configurations with charge transfer). The expression for calculation of $\langle f\rangle_{J-O}$ and $\langle f\rangle_{asci}$ values from corresponding line strengths is

$$\langle f\rangle = \frac{8\pi^2 m_e c}{3(2J+1)\bar{\lambda} h e^2} \frac{(n^2+2)^2}{9n} S(JJ'), \quad (4)$$

where n is the crystal refractive index at the wavelength of $\bar{\lambda}$.

Obtained values of $\langle f\rangle$ for ground-state absorption (GSA) channels are summarized in Table 2. ASCI approximation allows us to obtain lower root-mean-square (rms) deviation between experimental and calculated $\langle f\rangle$ values (0.14, compare with 1.35 for J–O theory). Similarly, absorption oscillator strengths were also determined for excited-state absorption (ESA) channels from metastable $^5D_0$ state, see Table 2. Strongest ESA processes are

related with $^5D_0 \rightarrow {}^5G_6$, $^5H_4$, $^5F_2$ and $^5F_4$ transitions. The last one corresponds to light wavelength of ~610 nm, the region of dominant emission of Eu^{3+} ions. The set of corresponding modeling parameters, namely {Ω_2, Ω_4 and Ω_6} for J–O theory and {O_{dk}, O_{ck}, Δ_d, Δ_{c1} and Δ_{c2}} for ASCI theory, is summarized in Table 3.

Overview of photoluminescence (PL) spectrum for Eu^{3+} ions in KYW crystal is shown in Fig. 5 (light polarization is $\boldsymbol{E}\|N_m$). Observed PL is related with radiative transitions from metastable $^5D_0$ state to lower-lying $^7F_{0-4}$ ones (the transition $^5D_0 \rightarrow {}^7F_2$ is the most intense). Moreover, weak but clearly-resolved band associated with relaxation from $^5D_1$ state to $^7F_2$ one (around 540 nm, marked with asterisk) is also detected. No blue broadband emission that is typically associated with partial reduction of Eu^{3+} ions to divalent form, Eu^{2+}, was observed in PL spectrum of Eu:KYW crystal. This indicates that Eu enters positions of Y^{3+} (C_2 cite) [20] in the host lattice.

Fig. 6 shows polarization-resolved structure of PL bands; their detailed characterization can be also found also in Table 1. On the basis of measured polarized PL spectra, stimulated-emission cross-sections σ_{em} were determined. For this, Fuchtbauer–Ladenburg equation [24] was utilized. The anisotropy of PL properties for Eu:KYW crystal is profound. It appears both in the shape of spectral bands and in their relative intensity. Indeed, the band associated with $^5D_0 \rightarrow {}^7F_4$ transition consists of two intense peaks centered at 702.6 and 705.8 nm (for $\boldsymbol{E}\|N_m$ and N_g); while for $\boldsymbol{E}\|N_p$ it contains one intense peak centered at 704.1 nm. This again agrees with the symmetry of Eu:KYW lattice, with N_m and N_g axes positioned in the plane orthogonal to N_p (C_2) one.

For principal light polarizations, peak stimulated-emission cross-sections take the relation $\sigma_{em}(m):\sigma_{em}(p):\sigma_{em}(g)=3.4:2.4:1$. Similar tendency is observed for band related with $^5D_0 \rightarrow {}^7F_2$ transition. In this case, the anisotropy is even higher, with $\sigma_{em}(m):\sigma_{em}(p):\sigma_{em}(g)=5.6:2.1:1$. Thus, from the point of Eu:KYW lasing, crystal orientation should provide access particularly to $\boldsymbol{E}\|N_m$ and N_p light polarizations. For $\boldsymbol{E}\|N_m$, peak stimulated-emission cross-section σ_{em} at the wavelengths of 613.4 and 702.1 nm is 4.02 and 1.34×10^{-20} cm^2, accordingly; FWHM of these peaks is ~1 nm.

Modeling of ESA (Table 2) indicates that peak wavelength of $^5D_0 \rightarrow {}^5F_4$ super-intense channel will correspond to the PL band associated with $^5D_0 \rightarrow {}^7F_2$ transition (similar conclusion was made also for highly-doped Eu:KGdW [13]). This is the main limitation for obtaining of laser operation at ~612 nm with Eu:KYW.

The ratio between integral intensities of bands associated with $^5D_0 \rightarrow {}^7F_2$ (electric dipole) and $^5D_0 \rightarrow {}^7F_1$ (magnetic dipole) transitions is defined as asymmetry parameter R. It is known to be the indicator of symmetry of Eu^{3+} site, as well as its distortion [25]. If the site has inversion center, the second band will be more intense. In another case, electric-dipole transition is dominant, showing higher crystal field strength. This is related with so-called short-range effects, namely increase of covalency and polarization of the local vicinities of Eu^{3+} cations.

According to our data, $R=12$ for bulk Eu:KYW (the intensity of bands was integrated over three principal light polarization) that agrees with previous data for isostructural Eu:KGdW. R parameter was determined for bulk ($R=10$ for 10 at% Eu) [13] and nanocrystalline Eu:KGdW (R~9 for 2 at% Eu and R~20–30 for stoichiometric $KEu_{0.5}Gd_{0.5}W$ and KEuW) [16]. One can see that asymmetry parameter enlarges substantially with the increase of Eu content in KGdW lattice that is related with increased site distortion. As the difference in the ionic radii of Y^{3+} and Eu^{3+} (1.019 and 1.066 Å) is larger than between Gd^{3+} and Eu^{3+} (1.053 and 1.066 Å), larger R value is expected for Eu:KYW than for Eu:KGdW (with the same Eu content).

Using set of parameters presented in Table 3, we calculated line strengths $S(JJ')$ for radiative spontaneous transitions from metastable $^5D_0$ state. On the basis of $S(JJ')$ values, the corresponding

Table 1
Peak wavelengths, λ_p, and corresponding absorption and emission cross-sections, σ_{abs} and σ_{em}, for $^7F_1 \rightarrow {}^5D_1$, $^5D_0 \rightarrow {}^7F_2$ and $^7F_4$ transitions for Eu^{3+} ion in $KY(WO_4)_2$ crystal.

Transition	Polarization	λ_p (nm)	σ_{abs} (10^{-20} cm^2)
Absorption			
$^7F_1 \rightarrow {}^5D_1$	$\boldsymbol{E}\|N_p$	534.3	0.48
		538.9	0.42
		540.0	0.26
	$\boldsymbol{E}\|N_m$	534.3	1.71
		540.0	0.62
	$\boldsymbol{E}\|N_g$	534.3	0.24
		540.0	0.08
Transition	Polarization	λ_p (nm)	σ_{em} (10^{-20} cm^2)
Stimulated-emission			
$^5D_0 \rightarrow {}^7F_2$	$\boldsymbol{E}\|N_p$	615.8	1.27
		617.5	1.53
	$\boldsymbol{E}\|N_m$	613.4	4.02
		619.2	2.37
	$\boldsymbol{E}\|N_g$	613.4	0.74
		619.2	0.51
$^5D_0 \rightarrow {}^7F_4$	$\boldsymbol{E}\|N_p$	704.1	0.93
	$\boldsymbol{E}\|N_m$	702.6	1.34
		705.8	0.60
	$\boldsymbol{E}\|N_g$	702.6	0.23
		705.8	0.39

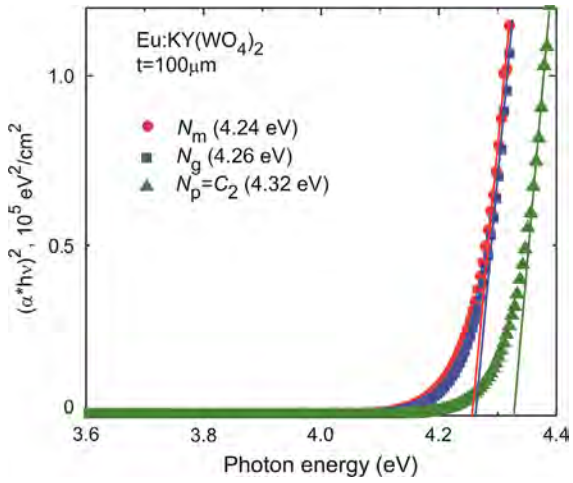

Fig. 4. Polarization-resolved Tauc plot for 2 at% $Eu:KY(WO_4)_2$ crystal.

Table 2
Polarization-averaged absorption oscillator strengths $\langle f_{exp}\rangle \times 10^6$ (determined from absorption spectra), $\langle f_{J-O}\rangle$ and $\langle f_{asci}\rangle \times 10^6$ (calculated by means of J–O and ASCI theories) for Eu^{3+} ion in $KY(WO_4)_2$ crystal.

GSA				ESA		
Transition	$\langle f\rangle_{exp}$	$\langle f\rangle_{J-O}$	$\langle f\rangle_{asci}$	Transition	$\langle f\rangle_{asci}$	$\langle\lambda\rangle$, nm
$^7F_{0,1} \rightarrow {}^7F_6$	6.74	8.58	6.74	$^5D_0 \rightarrow {}^5D_1$	0.7	
$^7F_5$	3.56	3.60	3.56	$^5D_2$	4.0	
$^7F_0 \rightarrow {}^5D_1$	0.09	0.03	0.03	$^5L_6$	31	
$^5D_2$	0.99	1.25	0.99	$^5G_2$	11	
$^5D_3$	0.05	–	–	$^5G_4$	25	1075
$^7F_1 \rightarrow {}^5D_0$	0.12	0.05	0.05	$^5G_6$	241	
$^5D_1$	1.33	1.18	1.35	$^5D_4$	19	
$^5D_2$	0.14	0.08	0.07	$^5H_4$	138	712
$^5D_3$	1.07	0.48	1.07	$^5H_6$	47	
$^7F_2 \rightarrow {}^5D_0$	1.87	–	–	$^5F_2$	194	629
$^7F_{0,1} \rightarrow {}^5L_6$	6.71	3.16	6.65	$^5F_4$	1829	610
RMS dev.		*1.35*	*0.14*			

probabilities of these transitions $A(JJ')$ are determined as:

$$A(JJ') = \frac{8\pi^2 n^2 e^2}{m_e c \bar{\lambda}^2} S(JJ'). \quad (5)$$

Thus, the branching ratios for luminescence from $^5D_0$ state and its radiative lifetime are

$$B(JJ') = \frac{A(JJ')}{\sum A(JJ')}, \quad (6a)$$

$$\tau_{rad} = \frac{1}{\sum A(JJ')}. \quad (6b)$$

Radiative lifetime τ_{rad} of $^5D_0$ state is 464 μs. For upper-lying $^5D_1$ state, it was determined in similar way to be 325 μs. The luminescence branching ratios B for $^5D_0 \rightarrow {}^7F_1$, $^7F_2$ and $^7F_4$ transitions are 0.033, 0.837 and 0.128, accordingly.

Main PL properties of 2 at% Eu:KYW crystal are summarized in Table 4.

PL decay curves for 2 at% Eu:KYW are presented in Fig. 7. The measurements are performed within three intense PL bands associated with transitions from $^5D_0$ to $^7F_1$, $^7F_2$ and $^7F_4$ states (at 595, 612 and 704 nm). The decay curves are clearly single-exponential. Luminescence decay time τ_{exp} equals 430 ± 10 μs. Thus, the $^5D_0$ state has the quantum efficiency close to unity. This is in agreement with the fact that higher phonon energy for KYW lattice is around 900 cm^{-1}. In addition, rise time of red PL was determined, being 4.1 μs. It is referred with the lifetime of $^5D_1$ state (as PL excitation is performed within $^7F_1 \rightarrow {}^5D_1$ channel). This time is substantially shorter than calculated radiative one (325 μs), mainly due to high non-radiative relaxation $^5D_1 \rightarrow {}^5D_0$ (the energy difference between these states is below 2000 cm^{-1}).

Previously, τ_{exp} was measured for several Eu-doped DTs compounds (Table 5), in the form of bulk crystal or nano-crystalline powder. The reported results cover the range of 0.2–1.5 ms, depending on host crystal, Eu content and material type. Our data are in good accordance with previous ones for isostructural bulk 10 and 25 at% Eu:KGdW (500 and 460 μs) [10,13]. However, the effect of substantial shortening of τ_{exp} for low doping ratio observed in Ref. [12] for bulk Eu:KLuW is not confirmed in the present paper.

Eu:doped DTs are known to be the appropriate phosphors for red and red-orange spectral region. In the present paper, we determine *Commission internationale de l'éclairage* (CIE)

Table 3
Parameters of J–O and ASCI theories applied for calculation of absorption oscillator strengths of Eu^{3+} ions in $KY(WO_4)_2$ crystal, see Eq. (3).

Theory, set of parameters	Value: 2 at% Eu^{3+}:$KY(WO_4)_2$
J–O theory: Ω_k [10^{-20} cm^2]	Ω_2=36.7, Ω_4=11.5, Ω_6=3.4
ASCI theory: O_{dk}, O_{ck} [10^{-10} cm], Δ_d, Δ_{c1} and Δ_{c2} [cm^{-1}]	O_{d2}=3.2, O_{d4}=3.0, O_{d6}=1.7, O_{c2}=−0.06, O_{c4}=0.08, O_{c6}=−0.08, Δ_d=37,000, Δ_{c1}=18,600, Δ_{c2}=26,500

Table 4
Summary of photoluminescent properties of Eu:$KY(WO_4)_2$ crystal.

Excitation peak/transition	394.8 nm/$^7F_0 \rightarrow {}^5L_6$
Emission peak/transition	613.4 nm/$^5D_0 \rightarrow {}^7F_2$
Luminescence branching ratios ($^5D_0 \rightarrow {}^7F_J$)	0.033 (J=1) 0.837 (J=2) 0.128 (J=4)
Asymmetry parameter R	12
Lifetime of $^5D_0$ state	430 μs (measured) 464 μs (radiative)
CIE coordinates	x=0.670, y=0.329
Color	Red
Dominant wavelength/purity	613 nm/98%

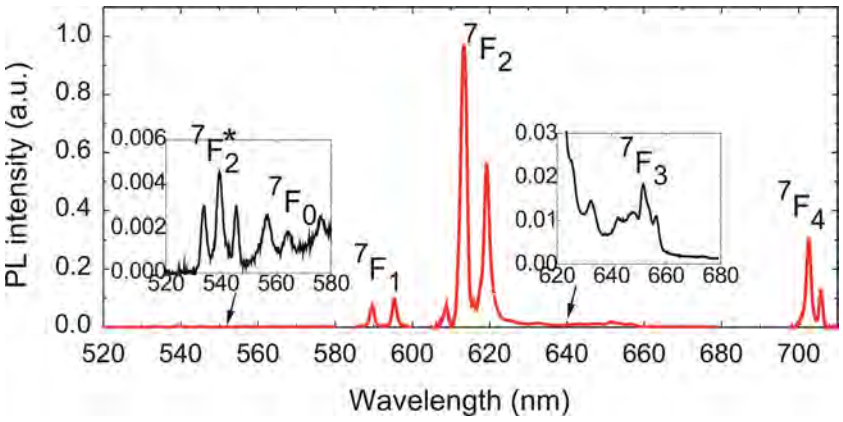

Fig. 5. Photoluminescence (PL) spectrum of 2 at% Eu:$KY(WO_4)_2$ crystal for light polarization $\boldsymbol{E}\|N_m$; excitation wavelength is 400 nm; all transitions occurs from $^5D_0$ state (*transition from $^5D_1$ state).

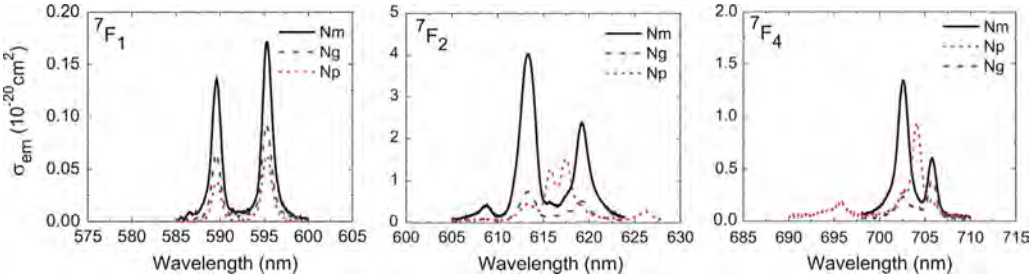

Fig. 6. Stimulated-emission spectra for Eu:$KGd(WO_4)_2$ crystal for light polarizations $\boldsymbol{E}\|N_p$, N_m, N_g: the bands associated with $^5D_0 \rightarrow {}^7F_{1,2,4}$ transitions are considered.

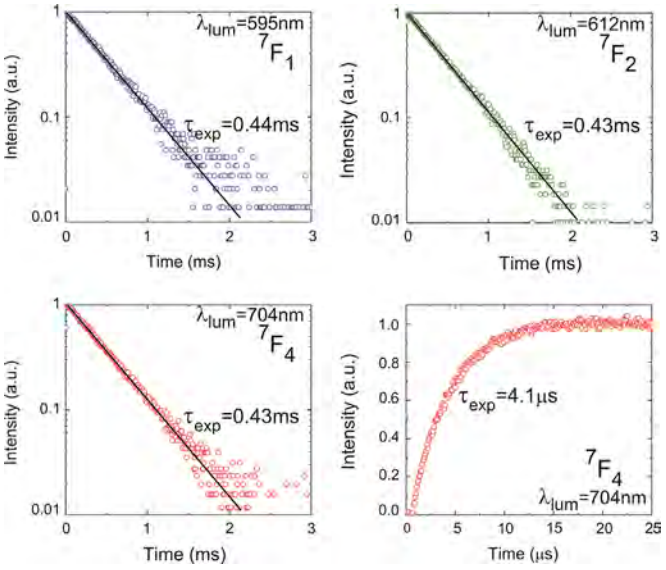

Fig. 7. Luminescence rise and decay curves for 2 at% Eu:KY$(WO_4)_2$; the $^5D_0 \rightarrow {}^7F_{1,2,4}$ transitions are considered; excitation wavelength is 400 nm.

Table 5
Measured lifetimes of $^5D_0$ state of Eu^{3+} ions in double tungstate (DT) compounds at room-temperature (RT).

Compound	Type	Eu content	τ (ms)	Ref.
$KGd(WO_4)_2$	Crystal	10 at%	0.50	[13]
		25 at%	0.46	[10]
	Phosphor	2 mol%	0.9–1.5	[15]
$KY(WO_4)_2$	Crystal	2 at%	0.43	This paper
$KYb(WO_4)_2$	Crystal	20 at%	0.21	[14]
	Phosphor	50 at%	0.23	[3]
	Phosphor	1 at%	0.7	[18]
$KLu(WO_4)_2$	Crystal	1 at%	0.26	[12]
		1.5 at%	0.68	
		3 at%	1.04	
		5 at%	1.29	
$NaLu(WO_4)_2$	Phosphor	5; 50 at%	0.54	[26]
$NaY(WO_4)_2$	Phosphor	1 mol%	1.0	[27]

Table 6
CIE coordinates for Eu-doped double tungstate (DT) compounds.

Compound	Eu content (at%)	Type	CIE (x,y)		Ref.
$KGd(WO_4)_2$	50	Phosphor	0.62	0.34	[28]
$KY(WO_4)_2$	2	Crystal	0.67	0.33	This paper
$KLu(WO_4)_2$	5	Crystal	0.59	0.35	[12]
$KYb(WO_4)_2$	50	Phosphor	0.68	0.32	[3]
$NaGd(WO_4)_2$	60	Phosphor	0.67	0.33	[29]
$NaY(WO_4)_2$	10	Phosphor	0.57	0.35	[30]
$NaEu(WO_4)_2$	–	Phosphor	0.66	0.34	[26]

coordinates for 2 at% Eu:KYW crystal, $x=0.670$ and $y=0.329$ that falls into the red region. The comparison with other DTs is performed in Table 6. The dominant wavelength in the PL spectrum is 613 nm with 98% purity. In the Eu:KREW family, the x coordinate increases in the row RE=Lu–Gd–Y–Yb (while y one is near constant ~0.32), that means shift from red-orange to red color. The CIE coordinates of Eu:KYW are similar to ones of disordered sodium DTs [26,29].

4. Conclusions

Large-volume 2 at% Eu:KY$(WO_4)_2$ is grown by top-seeded solution growth method. Absorption and stimulated-emission cross-section spectra are determined for this crystal with respect to principal light polarizations, $\boldsymbol{E}\|N_p$, N_m and N_g. Spectroscopic properties of Eu:KYW are modeled within conventional Judd–Ofelt theory, as well as theory of f–f transition intensities for systems with anomalously strong configuration interaction (ASCI), yielding absorption oscillator strengths (both for ground- and excited-state absorption), luminescence branching ratios and radiative lifetime of metastable $^5D_0$ state. PL decay and rise curves are measured for this crystal. It is predicted that $^5D_0 \rightarrow {}^5F_4$ super-intense ESA channel is the main limitation for obtaining of laser operation at ~612 nm with Eu:KYW. PL properties of Eu:KYW are determined. Under excitation by commercial InGaN laser diode (~400 nm), this crystal provides intense red emission with CIE coordinates $x=0.670$, $y=0.329$.

References

[1] G. Wakefield, E. Holland, P.J. Dobson, J.L. Hutchison, Adv. Mater. 13 (2001) 1557.
[2] S.L. Jones, D. Kumar, R.K. Singh, P.H. Holloway, Appl. Phys. Lett. 71 (1997) 404.
[3] M. Galceran, M.C. Pujol, P. Gluchowski, W. Strek, J.J. Carvajal, X. Mateos, M. Aguilo, F. Diaz, Opt. Mater. 32 (2010) 1493.
[4] Q. Shao, H. Li, K. Wu, Y. Dong, J. Jiang, J. Lumin. 129 (2009) 879.
[5] N.C. Chang, J. Appl. Phys. 34 (1963) 3500.
[6] E.J. Schimitschek, Appl. Phys. Lett. 3 (1963) 117.
[7] J.R. O'Conner, Trans. Metall. Soc. AIME 239 (1967) 362.
[8] J.H. Park, A.J. Steckl, J. Appl. Phys. 98 (2005) 056108.
[9] K. Nakamura, Y. Hasegawa, H. Kawai, N. Yasuda, N. Kanehisa, Y. Kai, T. Nagamura, S. Yanagida, Y. Wada, J. Phys. Chem. A 111 (2007) 3029.
[10] S.N. Bagaev, V.I. Dashkevich, V.A. Orlovich, S.M. Vatnik, A.A. Pavlyuk, A.M. Yurkin, Quantum Electron. 41 (2011) 189.
[11] V. Petrov, M.C. Pujol, X. Mateos, O. Silvestre, S. Rivier, M. Aguilo, R.M. Sole, J. Liu, U. Griebner, F. Diaz, Laser Photonics Rev 1 (2007) 179.
[12] M.C. Pujol, J.J. Carvajal, X. Mateos, R. Sole, J. Massons, M Aguilo, F Diaz, J. Lumin. 138 (2013) 77.
[13] P.A. Loiko, V.I. Dashkevich, S.N. Bagaev, V.A. Orlovich, A.S. Yasukevich, K.V. Yumashev, N.V. Kuleshov, E.B. Dunina, A.A. Kornienko, S.M. Vatnik, A.A. Pavlyuk, Laser Phys. 23 (2013) 105811-1.
[14] W. Strek, P.J. Deren, A. Bednarkiewicz, Y. Kalisky, P. Boulanger, J. Alloys Compd. 300–301 (2000) 180.
[15] R. Pazik, A. Zych, W. Strek, Mater. Chem. Phys. 115 (2010) 536.
[16] L. Macalik, P.E. Tomaszewski, R. Lisiecki, J. Hanuza, J. Solid State Chem. 131 (2008) 2591.
[17] X. Gao, Y. Wang, D. Wang, B. Liu, J. Lumin. 129 (2009) 840.
[18] A. Lukowiak, R.J. Wiglusz, R. Pazik, K. Lemanski, W. Strek, J. Rare Earth 27 (2008) 564.
[19] P.V. Klevtsov, L.P. Kozeeva, L.Yu. Kharchenko, Sov. Phys. Crystallogr. 20 (1975) 732.
[20] X. Mateos, R. Sole, Jna. Gavalda, M. Aguilo, J. Massons, F. Diaz, Opt. Mater. 28 (2006) 423.
[21] N. Thilmann, G. Strömqvist, M.C. Pujol, V. Pasiskevicius, V. Petrov, F. Díaz, Appl. Phys. B 96 (2009) 385.
[22] E.B. Dunina, A.A. Kornienko, L.A. Fomicheva, Cent. Eur. J. Phys. 6 (2008) 407.
[23] P.A. Loiko, A.S. Yasukevich, A.E. Gulevich, M.P. Demesh, M.B. Kosmyna, B.P. Nazarenko, V.M. Puzikov, A.N. Shekhovtsov, A.A. Kornienko, E.B. Dunina, N.V. Kuleshov, K.V. Yumashev, J. Lumin. 137 (2013) 252.
[24] B.F. Aull, H.P. Jenssen, IEEE J. Quantum Electron. 18 (1982) 925.
[25] A.F. Kirby, F.S. Richardson, J. Phys. Chem. 87 (1983) 2544.
[26] Z. Wang, H. Liang, Q. Wang, M. Chen, M. Gong, Q. Su, Phys. Status Solidi (a) 206 (2009) 1589.
[27] Y. Tian, B. Chen, R. Hua, N. Yu, B. Liu, J. Sun, L. Cheng, H. Zhong, X. Li, J. Zhang, B. Tian, H. Zhong, Cryst. Eng. Commun. 14 (2012) 1760.
[28] D. Thangaraju, A. Durairajan, D. Balaji, S. Moorthy Babu, Y Hayakawa, Mater. Chem. Phys. 135 (2012) 1115.
[29] J. Liao, H. You, B. Qiu, H.R. Wen, R. Hong, W. You, Z. Xie, Curr. Appl. Phys. 11 (2011) 503.
[30] X. Qian, X. Pun, D. Zhang, L. Li, M. Li, S. Wu, J. Lumin. 131 (2011) 1692.